



HAL
open science

Tunable magnetic anisotropy in Cr-trihalide Janus monolayers

Rehab Albaridy, Aurelien Manchon, Udo Schwingenschlögl

► **To cite this version:**

Rehab Albaridy, Aurelien Manchon, Udo Schwingenschlögl. Tunable magnetic anisotropy in Cr-trihalide Janus monolayers. *Journal of Physics: Condensed Matter*, 2020, 32 (35), pp.355702. 10.1088/1361-648x/ab8986 . hal-03033037

HAL Id: hal-03033037

<https://hal.science/hal-03033037>

Submitted on 1 Dec 2020

HAL is a multi-disciplinary open access archive for the deposit and dissemination of scientific research documents, whether they are published or not. The documents may come from teaching and research institutions in France or abroad, or from public or private research centers.

L'archive ouverte pluridisciplinaire **HAL**, est destinée au dépôt et à la diffusion de documents scientifiques de niveau recherche, publiés ou non, émanant des établissements d'enseignement et de recherche français ou étrangers, des laboratoires publics ou privés.

Tunable magnetic anisotropy in Cr–trihalide Janus monolayers

Rehab Albaridy, Aurelien Manchon  and Udo Schwingenschlögl 

Physical Sciences and Engineering Division (PSE), King Abdullah University of Science and Technology (KAUST), Thuwal, 23955-6900, Saudi Arabia

E-mail: udo.schwingenschlogl@kaust.edu.sa

Received 13 March 2020, revised 4 April 2020

Accepted for publication 15 April 2020

Published 29 May 2020



Abstract

Achieving a two-dimensional material with tunable magnetic anisotropy is highly desirable, especially if it is complemented with out-of-plane electric polarization, as this could provide a versatile platform for spintronic and multifunctional devices. Using first principles calculations, we demonstrate that the magnetic anisotropy of Cr–trihalides become highly sensitive to mechanical strain upon structural inversion symmetry breaking through the realization of Janus monolayers. This remarkable feature, absent in pristine Cr–trihalide monolayers, enables mechanical control of the direction of the easy axis: biaxial compressive/tensile strain supports in-plane/out-of-plane orientation of the easy axis. The magnetic exchange itself shows higher sensitivity to compressive than to tensile strain, while in general the Janus monolayers maintain ferromagnetic ordering in the studied range of strain.

Keywords: magnetic anisotropy, Janus monolayer, Cr–trihalide

 Supplementary material for this article is available [online](#)

(Some figures may appear in colour only in the online journal)

1. Introduction

Two dimensional (2D) materials can host inspiring features [1, 2], from spin–orbit physics leading to ultra-thin magnetic memories [3] to more exotic quantum spin liquid states [4] that could nurture futuristic topological quantum computing applications [5]. Relative ease of manipulating the mechanical, electronic, magnetic, and optical properties increases the possibilities to design 2D materials for a new generation of nanodevices [6–8]. In this context, it is of great interest to theoretically explore the potential of 2D ferromagnetic (FM) materials. Among the wide range of material candidates for 2D magnetism, transition metal trihalides stand out as a promising platform: following the prediction of FM ordering in monolayers of CrX₃ (X = Cl, Br, and I) [9], an experimental breakthrough confirmed FM ordering in a monolayer of CrI₃ with

a Curie temperature of 45 K [10] and boosted the interest in computational studies for this class of materials [11–16].

Monolayers of CrX₃ are non-metallic and based on bio-compatible trivalent chromium (Cr³⁺) [11]. It is attractive to achieve out-of-plane electric polarization in addition to the intrinsic magnetism, because this will open a new horizon in the field of multifunctional devices [17]. One way to reach this goal is by breaking the inversion symmetry of the monolayers, in which the Cr atoms are arranged in a honeycomb lattice sandwiched between planes of halide atoms forming a slightly distorted octahedral environment. When the two planes consist of different kinds of halide atoms the inversion symmetry is broken and out-of-plane electric polarization is obtained, leading to spin-momentum locking and thereby to an electrically-driven inverse spin galvanic effect, a photogalvanic effect, and Dzyaloshinski–Moriya interaction. This X₃–Cr₂–Y₃ (X, Y = Cl, Br, and I) structure is known as Janus monolayer. The Janus monolayer transition metal dichalcogenide MoSSe was recently demonstrated experimentally [18]. Janus Cr–trihalide monolayers are interesting for field-effect spin-filter applications [19] and possess a topological spin texture [20].



Original content from this work may be used under the terms of the [Creative Commons Attribution 4.0 licence](#). Any further distribution of this work must maintain attribution to the author(s) and the title of the work, journal citation and DOI.

Any magnetic 2D material must have magnetic anisotropy (MA), as at finite temperature thermal fluctuations destroy long range magnetic ordering according to the Mermin–Wagner theorem [21]. Uniaxial MA makes it possible to distinguish between two directions of magnetization, which can encode the values 0 and 1 for magnetic storage [22]. Possible applications in spintronics encourage search for novel methods to control the MA by external stimuli, such as mechanical deformations [23], exploiting anisotropic magnetostriction (i.e., a change of the magnetization direction causes a change of the material shape). The magnetostriction coefficient $\lambda = \frac{\Delta l}{l}$, where l is the length of the sample, is an important quantity from an application point of view. For example, small λ is desired for electric transformers and magnetic recorders, while large λ is attractive for microelectromechanical systems, sensors, and actuators [24]. The electronic and optical properties of 2D materials also can be strongly affected by strain [25–27]. In-plane strain can be achieved experimentally by epitaxial growth on a substrate with lattice mismatch (for example, a FeSe monolayer experiences 6% strain on SrTiO₃ [28]) and by mismatch between the thermal expansion coefficients of the 2D material and substrate (for example, up to 4.5% compressive strain on a Mo_{1-x}W_xS₂ monolayer on MgO [29]). In addition, the polymer-based encapsulation method makes it possible to exert controllable strain (for example, up to 6.5% strain on WSe₂ [30]).

Our work is inspired by the experiment of reference [31], in which the easy axis of the magnetization was tuned from in-plane (out-of-plane) to out-of-plane (in-plane) by varying the composition of CrCl_{3-x}Br_x from CrCl₃ to CrBr₃, raising the question about the origin of the modified easy axis. Is it just the composition or, maybe, an effect of strain or vacancies? Using first principles calculations, we investigate strain as one of the possible reasons considering the three Janus monolayers Cr₃–Cr₂–I₃, Br₃–Cr₂–I₃, and Cl₃–Cr₂–Br₃. First, we study the influence of the onsite Coulomb interaction U , finding that it is necessary to obtain correct results. Afterwards we calculate the mechanical properties and evaluate how much strain Cr–trihalides Janus monolayers can sustain as a precondition for investigating the effect of the strain on the structural, electronic, and magnetic properties. We apply strain from +5% to –5%, because this range is approachable experimentally and sufficient to understand the general pattern. We find for all three Janus monolayers planar structures that endure large strain. The broken inversion symmetry of Janus monolayers enhances the functionality by making the magnetic anisotropy highly sensitive to strain.

2. Results and discussion

2.1. Effect of the onsite Coulomb interaction

Bulk CrI₃ is an FM insulator with a Curie temperature of 61 K and has a layered rhombohedral structure, space group $R\bar{3}$, below 210–220 K. At higher temperature it has a monoclinic structure, space group C2/m, and is a paramagnetic insulator. A non-magnetic calculation using the generalized gradient

approximation (GGA) yields a metallic behaviour, contradicting the experimental result mentioned above. This indicates that the material is a Mott insulator, because the bandgap is not due to magnetic order but rather to electron–electron interaction [32]. Moreover, the FM ordering of bulk CrBr₃ and CrI₃ was reproduced by the GGA while the antiferromagnetic (AFM) ordering of bulk CrCl₃ can only be attained by taking into account an onsite Coulomb interaction within the around mean-field approach [33]. It is known that the local density approximation and GGA fail to capture Mott insulator properties, because they over-delocalize valence electrons [34]. Mott systems have strongly localized electrons and an onsite Coulomb interaction U thus can introduce a bandgap between the occupied and empty d states [23]. If U affects the structure relaxation, it causes significant changes in the hybridization between the d orbitals and their bonding partners, which directly influences the MA. As a matter of fact, this scenario applies to our Janus monolayers, as important features of the density of states (DOS) are affected by U , see the case of Cl₃–Cr₂–I₃ in figures 1(a) and (b): for the GGA the bandgap is between the occupied Cr t_{2g} and empty Cr e_g states, whereas in the GGA + U DOS it is between the occupied Br/I p states for Cl₃–Cr₂–Br₃/(Cl₃–Cr₂–I₃, Br₃–Cr₂–I₃) and the empty Cr e_g states (the Cr t_{2g} states have shifted below –1 eV). This may modify the effect of spin orbit coupling (SOC), which usually is determined by the orbitals near the Fermi level [35, 36], and thereby influences the magnetic properties. Thus, a proper treatment of the electronic states requires applying GGA + U calculations. Using the linear response approach, U was calculated for monolayers of CrCl₃, CrBr₃, and CrI₃ to be 2.65, 2.68, and 2.63 eV, respectively [11]. We use the average value for our Janus monolayers, $U = 2.65$ eV, which is justified, because the three values are very close to each other.

First, we test the influence of U for the pristine Cr–trihalide monolayers. We notice in table 1 as general pattern that U elongates all bonds, the easy axis becomes more in-plane, and the energy difference between FM and AFM ordering increases. This trend is particularly important when the energy difference is small, such as 13 meV in the case of monolayer CrBr₃ compressed by –5% strain, which is AFM when calculated without U but FM when calculated with U . Therefore, U can cause not only quantitative but also qualitative differences. The Janus monolayers turn out to follow the same trends as a function of U as the pristine monolayers, see table 2.

2.2. Mechanical properties

The elastic moduli are important physical parameters to evaluate whether a monolayer is mechanically stable, the equilibrium structure is planar or bended, and how much strain a monolayer can withstand. For sufficiently small stresses, the stress–strain (σ – ε) relationship is given by the generalized Hooke’s law, which can be expressed for a 2D hexagonal crystal as [6]

$$\begin{pmatrix} \sigma_{11} \\ \sigma_{22} \\ \sigma_{12} \end{pmatrix} = \begin{pmatrix} C_{11} & C_{21} & 0 \\ C_{12} & C_{22} & 0 \\ 0 & 0 & C_{66} \end{pmatrix} \begin{pmatrix} \varepsilon_{11} \\ \varepsilon_{22} \\ 2\varepsilon_{12} \end{pmatrix}, \quad (1)$$

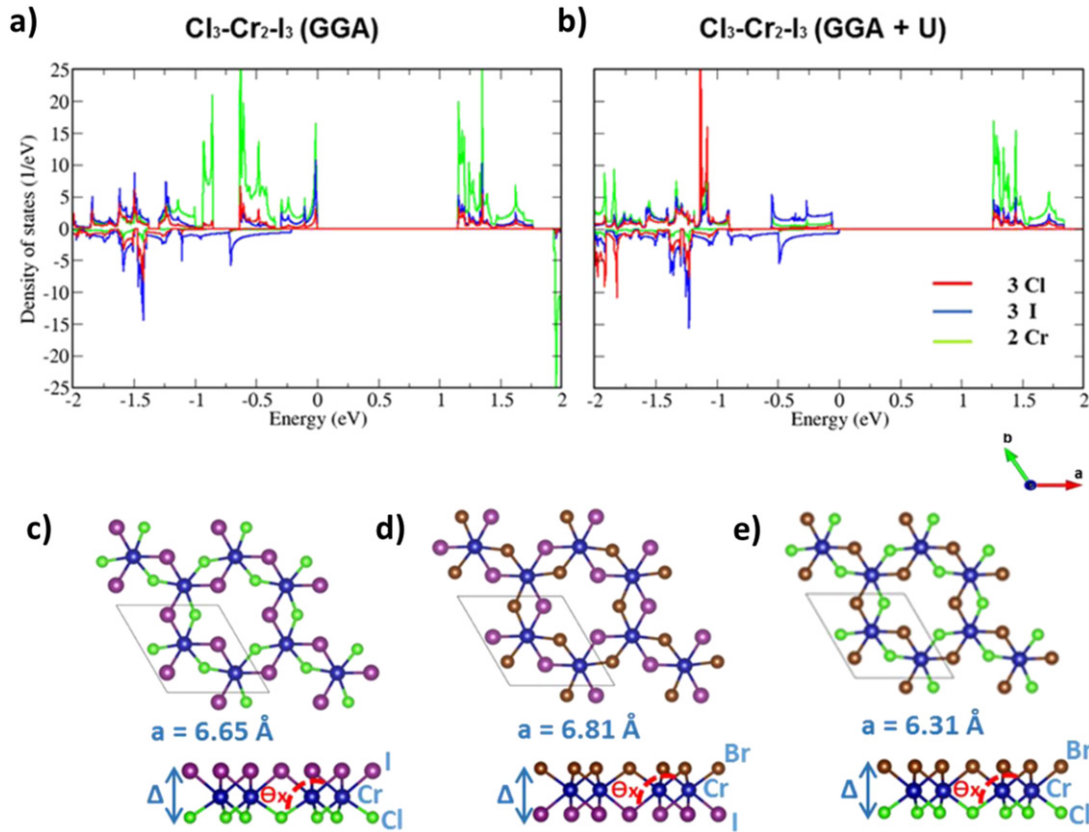


Figure 1. (a,b) Effect of the U parameter on the site-projected spin-polarized DOS of Cl₃-Cr₂-I₃. Top and side views of (c) Cl₃-Cr₂-I₃, (d) Br₃-Cr₂-I₃, and (e) Cl₃-Cr₂-Br₃ Janus monolayers.

Table 1. Calculated lattice constant (a), Cr-X/Cr-Cr bond lengths ($d_{\text{Cr-X}}/d_{\text{Cr-Cr}}$), exchange energy (E_{ex}), and magnetic anisotropy energy (MAE) for CrX₃ (X = I, Br, and Cl) under 0% strain, using the GGA and GGA + U methods.

| Monolayer | a (Å) | | $d_{\text{Cr-X}}$ (Å) | | $d_{\text{Cr-Cr}}$ (Å) | | E_{ex} (meV) | | MAE (meV) | |
|---|---------|-----------|-----------------------|-----------|------------------------|-----------|-----------------------|-----------|-----------|-----------|
| | GGA | GGA + U | GGA | GGA + U | GGA | GGA + U | GGA | GGA + U | GGA | GGA + U |
| I ₃ -Cr ₂ -I ₃ | 7.00 | 7.07 | 2.74 | 2.77 | 4.04 | 4.08 | 36 | 47 | 1.49 | 1.48 |
| Br ₃ -Cr ₂ -Br ₃ | 6.44 | 6.49 | 2.52 | 2.54 | 3.72 | 3.75 | 32 | 37 | 0.42 | 0.30 |
| Cl ₃ -Cr ₂ -Cl ₃ | 6.06 | 6.11 | 2.36 | 2.38 | 3.50 | 3.53 | 24 | 29 | 0.08 | 0.06 |

where C_{11} , C_{22} , C_{12} , C_{21} , and C_{66} are the elastic stiffness constants, defined as [37]

$$C_{11} = C_{22} = \frac{1}{A_0} \frac{\partial^2 E_s}{\partial \varepsilon_{11}^2}, \quad C_{12} = C_{21} = \frac{1}{A_0} \frac{\partial^2 E_s}{\partial \varepsilon_{11} \partial \varepsilon_{22}}$$

and

$$C_{66} = \frac{1}{A_0} \frac{\partial^2 E_s}{\partial \varepsilon_{12}^2} \quad (2)$$

Here A_0 is the equilibrium area, E_s is the strain energy (energy difference between the strained and unstrained systems, which depends quadratically on the applied strain, see figure 2), and the applied strain is defined as $\frac{a-a_0}{a_0}$, where a and a_0 are the lattice constants of the strained and unstrained systems, respectively. According to the Born criteria, $C_{11} > 1 \text{ N m}^{-1}$ and $C_{11} - C_{12} > 1 \text{ N m}^{-1}$ implies mechanical stability [38]. Our obtained values, as stated in table 3, satisfy these conditions.

To determine the stiffness of the Cr-trihalide Janus monolayers, Young's modulus is calculated from the elastic constants as [6]

$$Y_{2D} = \frac{C_{11}^2 - C_{12}^2}{C_{11}}. \quad (3)$$

According to table 3, Young's modulus of Cl₃-Cr₂-I₃, Br₃-Cr₂-I₃, and Cl₃-Cr₂-Br₃ is less than 10% of that of graphene (340 N m⁻¹) [39]. These small values imply that the Cr-trihalide Janus monolayers can be strained rather easily. Moreover, the out-of-plane deformation induced by gravity can be estimated by elastic theory as [40, 41]

$$\frac{h}{L} = \sqrt[3]{\frac{\rho g L}{Y_{2D}}}, \quad (4)$$

where L is the length of the flake, set to 100 μm, and ρ is the areal density, listed in table 3. We find $\frac{h}{L} = 4.3 \times 10^{-4}$, 4.8×10^{-4} , and 4.1×10^{-4} for Cl₃-Cr₂-I₃, Br₃-Cr₂-I₃,

Table 2. Calculated lattice constant (a), Cr–X/Cr–Y/Cr–Cr bond lengths ($d_{\text{Cr-X}}/d_{\text{Cr-Y}}/d_{\text{Cr-Cr}}$), exchange energy (E_{ex}), and magnetic anisotropy energy (MAE) for $\text{Y}_3\text{-Cr}_2\text{-X}_3$ (X, Y = I, Br, and Cl) under +5%, 0%, and –5% strain, using the GGA and GGA + U methods.

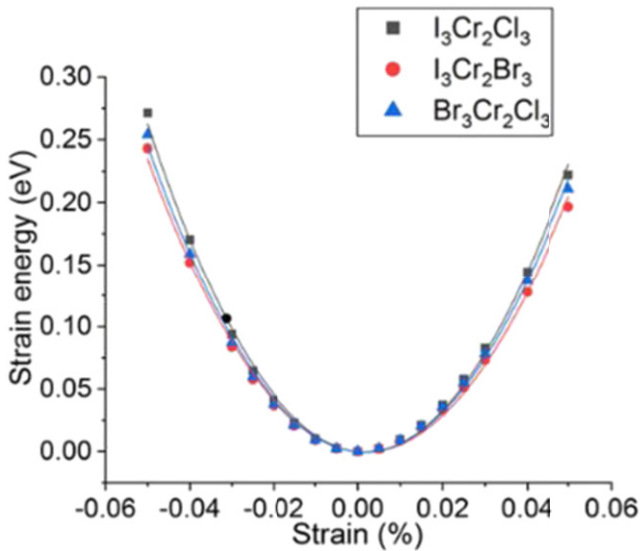
| $\text{Cl}_3\text{-Cr}_2\text{-I}_3$ | a (Å) | | $d_{\text{Cr-Cl}}$ (Å) | | $d_{\text{Cr-I}}$ (Å) | | $d_{\text{Cr-Cr}}$ (Å) | | E_{ex} (meV) | | MAE (meV) | |
|--------------------------------------|---------|-----------|------------------------|-----------|-----------------------|-----------|------------------------|-----------|-----------------------|-----------|-----------|-----------|
| | GGA | GGA + U | GGA | GGA + U | GGA | GGA + U | GGA | GGA + U | GGA | GGA + U | GGA | GGA + U |
| Strain +5% | 6.92 | 6.98 | 2.45 | 2.47 | 2.75 | 2.79 | 4.00 | 4.03 | 15 | 32 | 0.91 | 0.44 |
| Strain 0% | 6.59 | 6.65 | 2.40 | 2.42 | 2.71 | 2.74 | 3.81 | 3.84 | 24 | 32 | 0.18 | –0.84 |
| Strain –5% | 6.27 | 6.32 | 2.37 | 2.39 | 2.68 | 2.71 | 3.62 | 3.65 | 4 | 19 | –1.38 | –3.77 |

| $\text{Br}_3\text{-Cr}_2\text{-I}_3$ | a (Å) | | $d_{\text{Cr-I}}$ (Å) | | $d_{\text{Cr-Br}}$ (Å) | | $d_{\text{Cr-Cr}}$ (Å) | | E_{ex} (meV) | | MAE (meV) | |
|--------------------------------------|---------|-----------|-----------------------|-----------|------------------------|-----------|------------------------|-----------|-----------------------|-----------|-----------|-----------|
| | GGA | GGA + U | GGA | GGA + U | GGA | GGA + U | GGA | GGA + U | GGA | GGA + U | GGA | GGA + U |
| Strain +5% | 7.09 | 7.15 | 2.76 | 2.79 | 2.59 | 2.61 | 4.09 | 4.13 | 27 | 43 | 1.11 | 0.93 |
| Strain 0% | 6.75 | 6.81 | 2.72 | 2.75 | 2.54 | 2.57 | 3.90 | 3.93 | 32 | 41 | 0.85 | 0.16 |
| Strain –5% | 6.41 | 6.47 | 2.69 | 2.72 | 2.51 | 2.54 | 3.70 | 3.73 | 5 | 23 | 0.10 | –1.45 |

| $\text{Cl}_3\text{-Cr}_2\text{-Br}_3$ | a (Å) | | $d_{\text{Cr-Cl}}$ (Å) | | $d_{\text{Cr-Br}}$ (Å) | | $d_{\text{Cr-Cr}}$ (Å) | | E_{ex} (meV) | | MAE (meV) | |
|---------------------------------------|---------|-----------|------------------------|-----------|------------------------|-----------|------------------------|-----------|-----------------------|-----------|-----------|-----------|
| | GGA | GGA + U | GGA | GGA + U | GGA | GGA + U | GGA | GGA + U | GGA | GGA + U | GGA | GGA + U |
| Strain +5% | 6.58 | 6.63 | 2.41 | 2.43 | 2.55 | 2.57 | 3.80 | 3.83 | 25 | 31 | 0.40 | 0.32 |
| Strain 0% | 6.26 | 6.31 | 2.37 | 2.39 | 2.51 | 2.53 | 3.62 | 3.65 | 27 | 32 | 0.25 | 0.17 |
| Strain –5% | 5.95 | 5.99 | 2.34 | 2.36 | 2.48 | 2.50 | 3.43 | 3.46 | –21 | 9 | — | –0.04 |

Table 3. Elastic constants C_{11} and C_{12} , Young's modulus Y_{2D} , and areal density ρ .

| Monolayer | C_{11} (N m $^{-1}$) | C_{12} (N m $^{-1}$) | Y_{2D} (N m $^{-1}$) | ρ (kg m $^{-2}$) $\times 10^{-6}$ |
|---------------------------------------|-------------------------|-------------------------|-------------------------|---|
| $\text{I}_3\text{-Cr}_2\text{-I}_3$ | 25.5 [9] | 6.4 [9] | 23.8 [9] | 3.4×10^{-6} [9] |
| $\text{Br}_3\text{-Cr}_2\text{-Br}_3$ | 31.8 [9] | 8.8 [9] | 29.3 [9] | 2.7×10^{-6} [9] |
| $\text{Cl}_3\text{-Cr}_2\text{-Cl}_3$ | 37.3 [9] | 11.1 [9] | 34.0 [9] | 1.7×10^{-6} [9] |
| $\text{Cl}_3\text{-Cr}_2\text{-I}_3$ | 32.8 | 8.4 | 30.6 | 2.6×10^{-6} |
| $\text{Br}_3\text{-Cr}_2\text{-I}_3$ | 28.0 | 7.0 | 26.3 | 3.0×10^{-6} |
| $\text{Cl}_3\text{-Cr}_2\text{-Br}_3$ | 33.7 | 9.3 | 31.2 | 2.2×10^{-6} |

**Figure 2.** Variations of the strain energy under biaxial strain.

and $\text{Cl}_3\text{-Cr}_2\text{-Br}_3$, respectively. These values are of the same order of magnitude as in the case of graphene flakes of the same size [41], implying that Cr-trihalide Janus monolayers can withstand their own weight and keep a planar structure

without bending. Finally, figure 2 shows a small asymmetry of the strain energy as a function of the applied strain, implying that the application of tensile strain requires less energy than the application of compressive strain.

2.3. Crystal and electronic structure

Cr-trihalide Janus monolayers are structurally stable [14] and share a hexagonal structure, see figures 1(c–e). As the octahedral crystal field splits the Cr d orbitals into three occupied t_{2g} orbitals and two empty e_g orbitals, the Cr magnetic moments turn out to be approximately $3 \mu_B$ ($4s^0 3d^3$ electronic configuration), where the halide ions show a residual counter-magnetization of at most $0.16 \mu_B$. The crystal field splitting is larger when the Cr oxidation state is higher and/or the electronegativity of the halide is higher [42]. This is the reason why the bandgaps of $\text{Cl}_3\text{-Cr}_2\text{-I}_3$ and $\text{Br}_3\text{-Cr}_2\text{-I}_3$ are smaller than the bandgap of $\text{Cl}_3\text{-Cr}_2\text{-Br}_3$, as I has lower electronegativity than Br and Cl. In each case the bandgap is indirect, as shown in figure 3. The top of the valence band is dominated by the p states of the halide atom with lower electronegativity, i.e., I for $\text{Cl}_3\text{-Cr}_2\text{-I}_3$ and $\text{Br}_3\text{-Cr}_2\text{-I}_3$, and Br for $\text{Cl}_3\text{-Cr}_2\text{-Br}_3$. The bottom of the conduction band is dominated by the Cr d states. These contributions are demonstrated in figure 3 for the

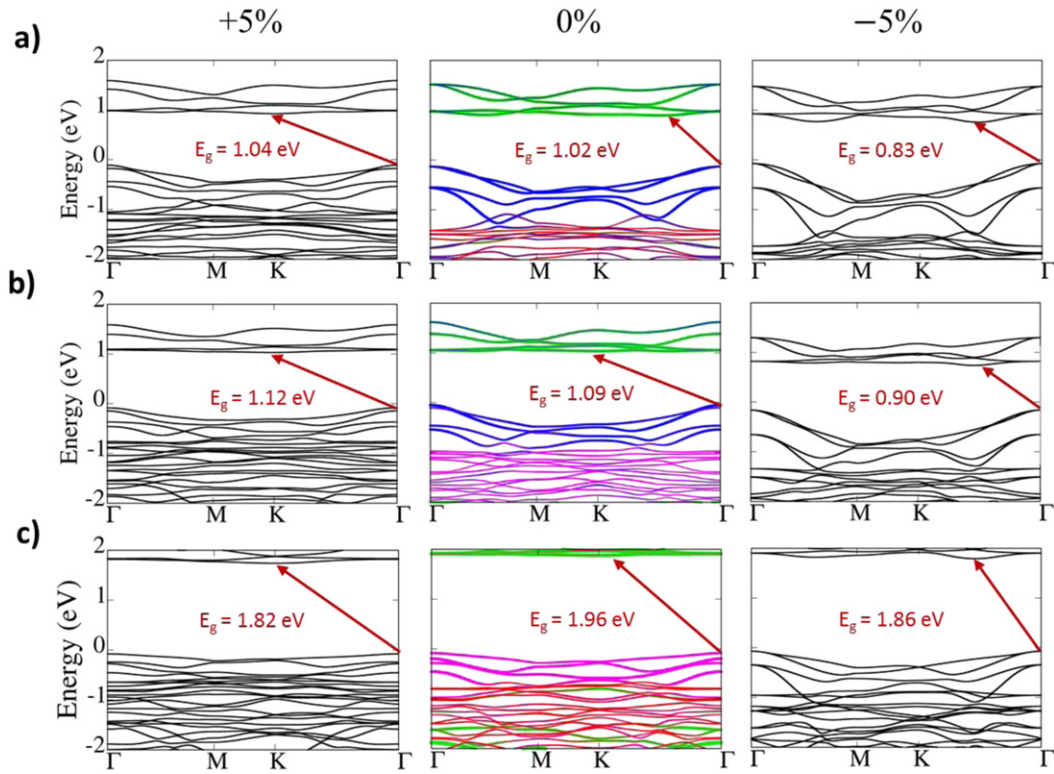


Figure 3. Band structures taking into account SOC for (a) $\text{Cl}_3\text{-Cr}_2\text{-I}_3$, (b) $\text{Br}_3\text{-Cr}_2\text{-I}_3$, and (c) $\text{Cl}_3\text{-Cr}_2\text{-Br}_3$, where +5%, 0%, and -5% strain is applied. The red, green, blue, and magenta colors represent the weights of the Cl, Cr, I, and Br atoms, respectively. Red arrows represent the indirect band gap.

Table 4. Calculated lattice constant (a), Cr-X/Cr-Y/Cr-Cr bond lengths ($d_{\text{Cr-X}}/d_{\text{Cr-Y}}/d_{\text{Cr-Cr}}$), interlayer vertical distance between X and Y (Δ), Cr-X-Cr/Cr-Y-Cr bond angles ($\Theta_{\text{Cr-X-Cr}}/\Theta_{\text{Cr-Y-Cr}}$), and axial bond angle (Θ_x).

| $\text{Cl}_3\text{-Cr}_2\text{-I}_3$ | a (Å) | $d_{\text{Cr-Cl}}$ (Å) | $d_{\text{Cr-I}}$ (Å) | $d_{\text{Cr-Cr}}$ (Å) | Δ (Å) | $\Theta_{\text{Cr-Cl-Cr}}$ (°) | $\Theta_{\text{Cr-I-Cr}}$ (°) | Θ_x (°) |
|---------------------------------------|---------|------------------------|------------------------|------------------------|--------------|--------------------------------|--------------------------------|----------------|
| Strain +5% | 6.98 | 2.47 | 2.79 | 4.03 | 2.86 | 109 | 93 | 168 |
| Strain 0% | 6.65 | 2.42 | 2.74 | 3.84 | 2.93 | 105 | 89 | 170 |
| Strain -5% | 6.32 | 2.39 | 2.71 | 3.65 | 3.03 | 99 | 85 | 172 |
| $\text{Br}_3\text{-Cr}_2\text{-I}_3$ | a (Å) | $d_{\text{Cr-I}}$ (Å) | $d_{\text{Cr-Br}}$ (Å) | $d_{\text{Cr-Cr}}$ (Å) | Δ (Å) | $\Theta_{\text{Cr-I-Cr}}$ (°) | $\Theta_{\text{Cr-Br-Cr}}$ (°) | Θ_x (°) |
| Strain +5% | 7.15 | 2.79 | 2.61 | 4.13 | 2.97 | 95 | 104 | 169 |
| Strain 0% | 6.81 | 2.75 | 2.57 | 3.93 | 3.04 | 91 | 100 | 172 |
| Strain -5% | 6.47 | 2.72 | 2.54 | 3.73 | 3.13 | 87 | 95 | 175 |
| $\text{Cl}_3\text{-Cr}_2\text{-Br}_3$ | a (Å) | $d_{\text{Cr-Cl}}$ (Å) | $d_{\text{Cr-Br}}$ (Å) | $d_{\text{Cr-Cr}}$ (Å) | Δ (Å) | $\Theta_{\text{Cr-Cl-Cr}}$ (°) | $\Theta_{\text{Cr-Br-Cr}}$ (°) | Θ_x (°) |
| Strain +5% | 6.63 | 2.43 | 2.57 | 3.83 | 2.73 | 104 | 96 | 170 |
| Strain 0% | 6.31 | 2.39 | 2.53 | 3.65 | 2.80 | 99 | 92 | 173 |
| Strain -5% | 5.99 | 2.36 | 2.50 | 3.46 | 2.89 | 94 | 88 | 176 |

case of 0% strain and the structural changes under strain are summarized in table 4.

An interesting feature is noted for the size of the bandgap E_g in the strain range from -2% to +2%: for $\text{Cl}_3\text{-Cr}_2\text{-I}_3$ and $\text{Br}_3\text{-Cr}_2\text{-I}_3$ it decreases under compression and increases under tension, whereas for $\text{Cl}_3\text{-Cr}_2\text{-Br}_3$ it follows the opposite trend, as elucidated by figure 4. SOC cannot explain this observation, because it only decreases E_g but does not alter the general behaviour under strain. However, the observation can be explained by competing effects of the band

width (orbital overlap) and crystal field splitting. Under compression/tension the former decreases/increases and the latter increases/decreases E_g . Accordingly, one can conclude that $\text{Cl}_3\text{-Cr}_2\text{-I}_3$ and $\text{Br}_3\text{-Cr}_2\text{-I}_3$ are dominated by the alteration of the band width, whereas $\text{Cl}_3\text{-Cr}_2\text{-Br}_3$ is dominated by the modification of the crystal field splitting.

2.4. Magnetic properties

In Cr-trihalide Janus monolayers the two magnetic Cr atoms interact through a non-magnetic halide atom by

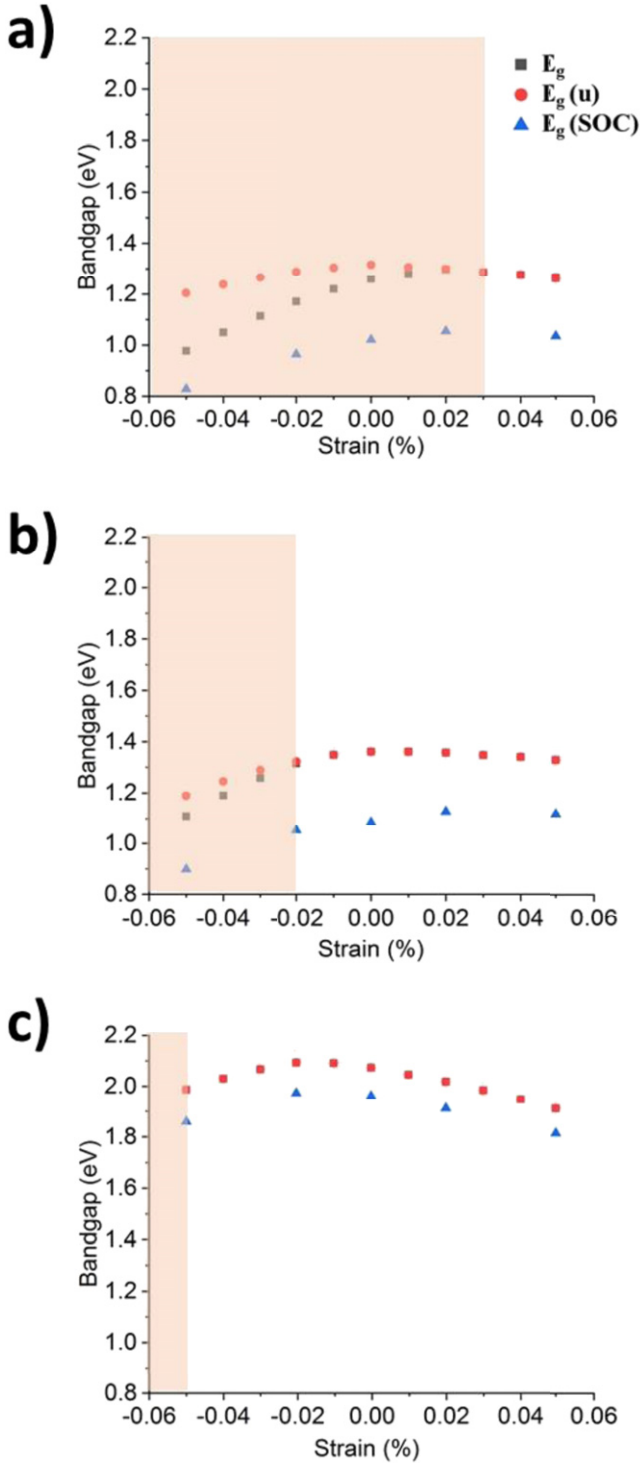


Figure 4. Variations of the bandgap E_g without SOC, bandgap E_g (u) of the spin up channel without SOC, and bandgap E_g (SOC) with SOC under strain for (a) $\text{Cl}_3\text{-Cr}_2\text{-I}_3$, (b) $\text{Br}_3\text{-Cr}_2\text{-I}_3$, and (c) $\text{Cl}_3\text{-Cr}_2\text{-Br}_3$. In the highlighted region the easy axis is in-plane.

superexchange. The Goodenough–Kanamori–Anderson rules establish the sign of the superexchange constant [43]. All monolayers under study satisfy these rules for FM superexchange, because the d orbitals of the magnetic atoms are half occupied and form an angle of approximately 90° with the halide atoms. A recent study [16] has shown, using the Green’s function method, that the halide atoms play a vital

role in the FM ordering of CrCl_3 and CrI_3 , because when their spin-polarization is neglected the ordering becomes AFM. In the strain range from +5% to –5% all the Cr–trihalide Janus monolayers maintain FM ordering. However, we find that compression decreases the energy difference between FM and AFM ordering (exchange energy $E_{\text{ex}} = E_{\text{FM}} - E_{\text{AFM}}$), see table 5. Therefore, we expect a transition to AFM ordering when the compression is further increased. On the other hand, tension alters E_{ex} only little. This can be explained by competition between direct exchange through Cr–Cr bonding, which leads to AFM ordering, and superexchange through Cr–X–Cr bonding, which leads to FM ordering. The Cr–Cr bonding is more sensitive to the strain than the Cr–X bonding, compare the influence of strain on the bond lengths given in table 4. Moreover, the Cr–X–Cr bond angle barely changes under strain, see table 4, which points to a low impact of strain on the superexchange. To calculate E_{ex} , we consider the energies of FM and AFM orderings and fit them to the nearest neighbour Heisenberg spin Hamiltonian (localized spin system)

$$H = - \sum_{i,j} J \vec{S}_i \cdot \vec{S}_j, \quad (5)$$

where J is the exchange constant, \vec{S}_i/\vec{S}_j is the spin at lattice site i/j , and the sum includes only nearest neighbours [22]. This implies $E_{\text{FM}} = E_0 - 3J|\vec{S}|^2$ and $E_{\text{AFM}} = E_0 + 3J|\vec{S}|^2$, and further $J = -\frac{2}{27}E_{\text{ex}}$. The obtained values of J are summarized in table 5.

The magnetic anisotropy energy (MAE) depends on the SOC, known as magneto crystalline anisotropy, and the dipole–dipole interaction, known as shape anisotropy [24]. The MAE is the total energy difference between in-plane and out-of-plane magnetization. When it is negative/positive the easy axis is oriented in-plane/out-of-plane. As non-collinear calculations performed by the Vienna *ab initio* simulation package (VASP) do not distinguish between easy and hard axes when SOC is not included [44], it is not possible to obtain the dipole–dipole contribution to the MAE. Fortunately, the magneto crystalline anisotropy dominates the MAE in low dimensional systems [22], i.e., we can relate our results to the effect of SOC only. The contribution of SOC to the Hamiltonian is [23]

$$H^{\text{SOC}} = -\frac{e\hbar^2}{2m_e^2c^2} \frac{d\Phi(r)}{rdr} (\vec{S} \cdot \vec{L}) = \xi_r (\vec{S} \cdot \vec{L}), \quad (6)$$

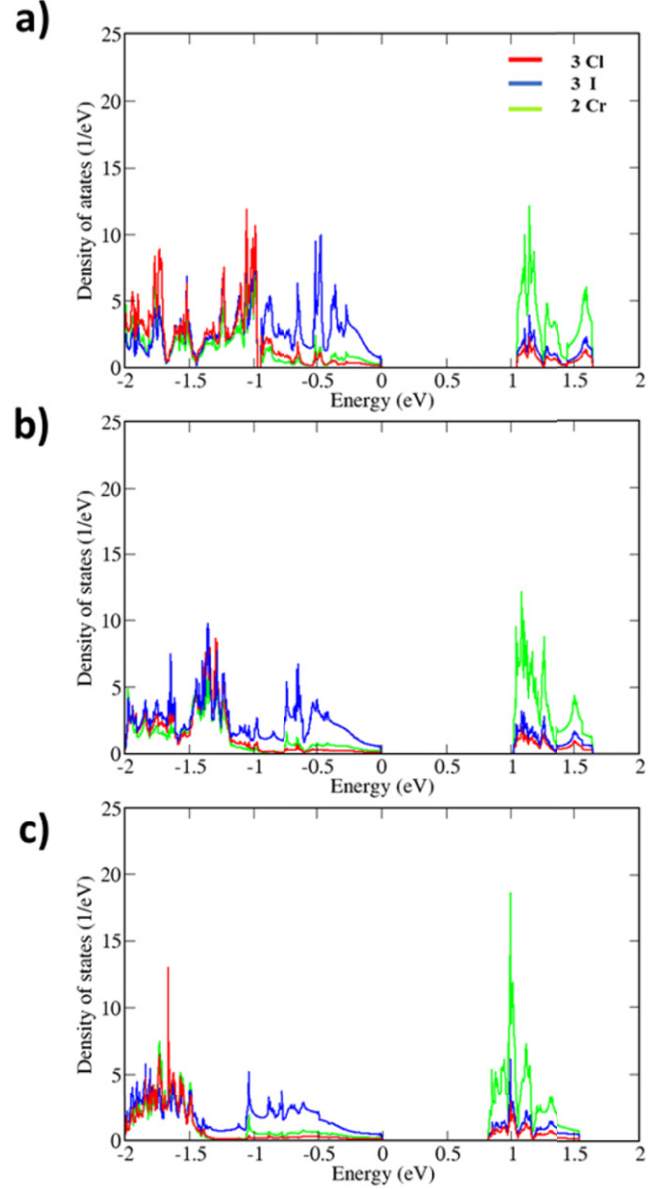
where \vec{L} is the total orbital angular momentum and $\Phi(r) = \frac{Ze}{4\pi\epsilon_0 r}$ the electrostatic potential of the nucleus. The SOC constant ξ_r is considered to be an atomic property (hardly changes from the free atom to a crystal), because the derivative is largest close to the nucleus [45]. It is roughly proportional to the square of the atomic number Z [22]. Table 5 indicates that compression/tension decreases/increases the MAE, i.e., compression destabilizes an out-of-plane easy axis and promotes an in-plane easy axis. This can be explained qualitatively in terms of the Cr–X and Cr–Y bond lengths. According to table 4, both bond lengths decrease under compression, while the thickness Δ , as defined in figures 1(c–e), increases. This means that the in-plane component of the Cr d orbitals is more sensitive to the strain than the out-of-plane component. Disturbance of

Table 5. Exchange energy (E_{ex}), exchange constant (J), and magnetic anisotropy energy (MAE).

| Monolayer | Strain +5% | | | Strain 0% | | | Strain -5% | | |
|---|-----------------------|-----------|-----------|-----------------------|-----------|-----------|-----------------------|-----------|-----------|
| | E_{ex} (meV) | J (meV) | MAE (meV) | E_{ex} (meV) | J (meV) | MAE (meV) | E_{ex} (meV) | J (meV) | MAE (meV) |
| Cl ₃ -Cr ₂ -I ₃ | -31.56 | 2.34 | 0.44 | -32.33 | 2.39 | -0.84 | -18.99 | 1.41 | -3.77 |
| Br ₃ -Cr ₂ -I ₃ | -42.80 | 3.17 | 0.93 | -40.90 | 3.04 | 0.16 | -23.30 | 1.73 | -1.45 |
| Cl ₃ -Cr ₂ -Br ₃ | -30.78 | 2.28 | 0.32 | -32.47 | 2.41 | 0.17 | -9.10 | 0.67 | -0.04 |
| I ₃ -Cr ₂ -I ₃ | -51.12 | 3.79 | 1.75 | -47.05 | 3.49 | 1.48 | -28.20 | 2.09 | 1.62 |
| Br ₃ -Cr ₂ -Br ₃ | -37.52 | 2.78 | 0.47 | -37.16 | 2.75 | 0.30 | -14.33 | 1.06 | 0.15 |
| Cl ₃ -Cr ₂ -Cl ₃ | -27.75 | 2.06 | 0.15 | -28.95 | 2.14 | 0.06 | 2.17 | -0.16 | -0.05 |

the in-plane motion of the electrons causes a reduction of the out-of-plane component of \vec{L} [23]. Because the easy axis is determined by the direction of \vec{L} , it is oriented in-plane/out-of-plane when \vec{L} points predominantly in-plane/out-of-plane. Therefore, compression destabilizes an out-of-plane easy axis until an in-plane easy axis is achieved, and tension has the opposite effect. Figure 5 shows the site-projected DOS for Cl₃-Cr₂-I₃ in the cases of +5%, 0%, and -5% strain. We observe that the band width of the Cr-dominated conduction band (which consists of both in-plane and out-of-plane components of the Cr d orbitals) increases (0.60 eV, 0.63 eV, and 0.72 eV at +5%, 0%, and -5% strain, respectively). The out-of-plane component cannot be the cause of this increase, as Δ increases. Thus, the increased band width must be due to the fact that the in-plane component of the d orbitals interacts more with the halide orbitals, as the bond length decreases. This causes disturbance of the in-plane motion of the electrons. An exception is monolayer CrI₃ where the MAE increases under both compression and tension. The single ion anisotropy of Cr can play a role in explaining this behaviour, because strain increases its contribution to the MAE depending on the type of atoms involved, whereas its contribution to the MAE can be neglected for unstrained CrI₃, as shown in reference [12], and the MAE is dominated by the SOC of I through superexchange. Single ion anisotropy can also explain why the MAE under -5% strain follows the trend Cl₃-Cr₂-Br₃ < Br₃-Cr₂-I₃ < Cl₃-Cr₂-I₃, i.e., the same trend as the difference in the electronegativity between the involved atoms, $\chi_{\text{Cl}} - \chi_{\text{Br}} < \chi_{\text{Br}} - \chi_{\text{I}} < \chi_{\text{Cl}} - \chi_{\text{I}}$. On the other hand, under +5% strain the SOC of I through superexchange seems to be dominant, as the MAE increases with the mass of the involved atoms as Cl₃-Cr₂-Br₃ < Cl₃-Cr₂-I₃ < Br₃-Cr₂-I₃.

Applying strain to Cr-trihalide Janus monolayers gives rise to three unique features not available in the pristine monolayers. Firstly, the ability to switch the easy axis by a small amount of strain. For example, Cl₃-Cr₂-I₃ switches from in-plane to out-of-plane easy axis at +3% strain and Br₃-Cr₂-I₃ switches from out-of-plane to in-plane easy axis at -2% strain. On the other hand, monolayer CrI₃ and CrBr₃ do not lose their out-of-plane easy axis even under $\pm 10\%$ strain [46]. Secondly, Cl₃-Cr₂-I₃ has a very negative (in-plane) MAE under -5% strain, -3.77 meV per formula unit. Thirdly, all the studied Cr-trihalide Janus monolayers maintain FM ordering during the switching, while in the case of the pristine Cr-trihalide monolayers the easy axis switches at the phase transition from

**Figure 5.** Site-projected DOS with SOC under strains of (a) +5%, (b) 0%, and (c) -5% for Cl₃-Cr₂-I₃.

FM to AFM ordering, as shown for monolayer CrCl₃ in table 5 and previously in reference [46].

Assuming that there are only two-fold symmetries, which dominate in low-dimensional systems, the MAE of a perfect

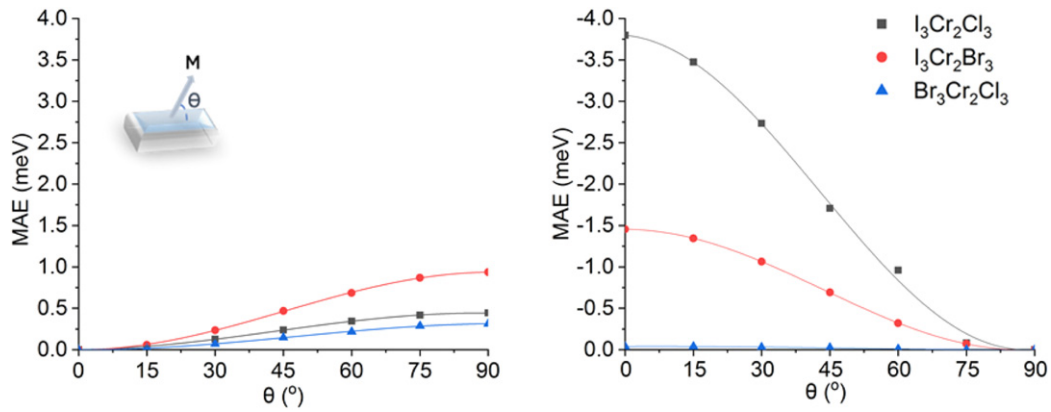


Figure 6. Variations of the MAE (per formula unit) with θ at (a) +5% strain and (b) -5% strain. The lines are obtained by fitting the data as $A\sin^2\theta$.

thin film is given by [22]

$$E_{\text{MAE}} = K_{zz} \sin^2 \theta, \quad (7)$$

where θ is the angle between the direction of magnetization and the 2D plane, and K_{zz} is the single-site anisotropy constant (positive/negative for out-of-plane/in-plane easy axis). Figure 6 shows for all three Cr-trihalide Janus monolayers that at maximum strain ($\pm 5\%$) the MAE follows the angular dependence $\sin^2\theta$, except for the case of $\text{Cl}_3\text{-Cr}_2\text{-Br}_3$ at -5% strain, where it is very small and the accuracy of the calculation is not sufficient to decide the functional dependence. Yet, the data do not contradict a $\sin^2\theta$ dependence. It is worth to mention an observation that enables us to predict the easy axis without SOC calculations (both with and without U). As shown in figure 4, when the bandgap opens up between states of identical/different spin the preferable direction of the easy axis is out-of-plane/in-plane. Also, we find that for decreasing/increasing spin splitting of the valence band near the Fermi level the value of the MAE decreases/increases. Again there is an exception to this rule: $\text{Cl}_3\text{-Cr}_2\text{-Br}_3$ under compression. The reason can be the strong crystal field splitting or the fact that the SOC in this case has two comparably strong sources, the Br p orbitals and Cr d orbitals, as ξ_r is of the same order of magnitude for Br and Cr. Consequently, Br is not the dominating source of the SOC in contrast to $\text{Cl}_3\text{-Cr}_2\text{-I}_3$ and $\text{Br}_3\text{-Cr}_2\text{-I}_3$, where I dominates over Cr, as shown previously for monolayer CrI_3 [12].

3. Conclusion

We have used GGA + U calculations to investigate the structural properties, magnetic properties, and electronic states of the Cr-trihalide Janus monolayers $\text{X}_3\text{-Cr}_2\text{-Y}_3$ ($\text{X}, \text{Y} = \text{Cl}, \text{Br}, \text{and I}$) under strain in the range from -5% to $+5\%$. All three Janus monolayers maintain a planar (non-bended) structure and have small Young's moduli, which means that the application of large strain is experimentally possible. Both the pristine CrX_3 ($\text{X} = \text{Cl}, \text{Br}, \text{and I}$) and Cr-trihalide Janus monolayers turn out to be Mott insulators, i.e., the onsite Coulomb interaction is essential to be taken into account in the calculations, as it changes the physical properties qualitatively. FM ordering

turns out to be the ground state for all three Cr-trihalide Janus monolayers in the studied range of strain, even though the energy difference between FM and AFM ordering decreases for increasing compressive strain. Having a strain-tunable bandgap, a remarkable feature of the Cr-trihalide Janus monolayers pertains to the high sensitivity of their MAE to mechanical strain. Our calculations show that small strain up to -2% can lead to anisotropy switching from out-of-plane to in-plane, while maintaining the FM ordering. This feature is absent in the pristine Cr-trihalide monolayers. Compressive strain favours an in-plane easy axis, whereas tensile strain favours an out-of-plane easy axis. The MAE of $\text{Cl}_3\text{-Cr}_2\text{-I}_3$ reaches a very negative value of -3.77 meV per formula unit under -5% strain. The fact that the availability of Janus monolayers with lattice constants and material properties different from those of the pristine monolayers increases the choices to engineer 2D van der Waals magnetic heterostructures creates a venue to provide spintronic and valleytronic materials with desired properties. For example, it was demonstrated that the spin and valley pseudospin can be controlled magnetically in a heterostructure consisting of an ultrathin CrI_3 film on top of WSe_2 [47]. In addition, van der Waals stacking can be used to raise the Curie temperature to room temperature, which was achieved experimentally for a $\text{EuS-Bi}_2\text{Se}_3$ heterostructure (Curie temperature of EuS rises from 17 K to 300 K) [48]. This finding was explained theoretically by the presence of topological surface states at the $\text{EuS-Bi}_2\text{Se}_3$ interface [49]. It is also interesting to study Dzyaloshinski-Moriya interaction in Cr-trihalide Janus monolayers, $H_{\text{DM}} = \sum_{i,j} \vec{D}_{i,j} \cdot (\vec{S}_i \times \vec{S}_j)$, where $\vec{D}_{i,j}$ is governed by the symmetry of the system and depends on the real space direction given by sites i and j [22], because the Cr-trihalide Janus monolayers combine SOC, absence of time-reversal symmetry, and broken inversion symmetry (gradient of the electric potential normal to the surface). As a consequence, the electron hopping from site i to site j is not equivalent to the hopping from site j to site i , leading to the onset of Dzyaloshinski-Moriya interaction, which can stabilize homochiral, helical, and cycloidal spin spirals [50, 51]. All these properties make the Cr-trihalide Janus monolayers promising for spintronic and multifunctional devices.

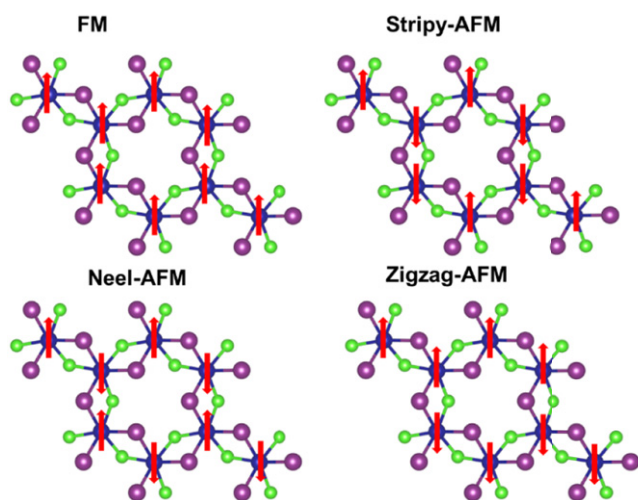


Figure 7. Magnetic orderings considered in the calculations.

3.1. Computational details

The first principles calculations in this work were performed using the projector augmented wave method as implemented in VASP [52]. We applied the Perdew–Burke–Ernzerhof parametrization [53] of the GGA for the exchange correlation functional, taking into account an onsite Coulomb interaction U [54] to accurately describe the Cr 3d states. The Brillouin zone was sampled on a Γ -centred Monkhorst–Pack $16 \times 16 \times 1$ k -mesh, with a total energy difference of less than 0.002 meV to a $20 \times 20 \times 1$ k -mesh. The plane wave cutoff energy was set to 800 eV, with a total energy difference of less than 0.025 meV (0.058 meV) for the Cr–trihalide Janus monolayers (for the pristine Cr–trihalide monolayers) to a 900 eV cutoff energy. The atomic structures were carefully relaxed until the Hellmann–Feynman forces on each atom became smaller than $0.005 \text{ eV } \text{\AA}^{-1}$. We introduced a layer of vacuum of at least 18 \AA thickness in the z -direction to avoid interaction between periodic images, i.e., to model a 2D system. The MAE was determined by 1) spin polarized calculations (collinear) for the FM and AFM orderings shown in figure 7 followed by 2) SOC calculations (non-collinear) for the FM ground state, all performed with full atomic relaxation, to obtain the total energy difference between in-plane and out-of-plane magnetization.

Acknowledgements

The authors thank Dr Xiaoning Zang and Dr Shahid Sattar for fruitful discussions. The research reported in this publication was supported by funding from King Abdullah University of Science and Technology (KAUST).

ORCID iDs

Aurelien Manchon  <https://orcid.org/0000-0002-4768-293X>

Udo Schwingenschlöggl  <https://orcid.org/0000-0003-4179-7231>

References

- [1] Dresselhaus M S and Dresselhaus G 2002 Intercalation compounds of graphite *Adv. Phys.* **51** 1–186
- [2] Dean C R *et al* 2013 Hofstadter’s butterfly and the fractal quantum Hall effect in Moiré superlattices *Nature* **497** 598–602
- [3] Manchon A, Železný J, Miron I M, Jungwirth T, Sinova J, Thivaille A, Garello K and Gambardella P 2019 Current-induced spin–orbit torques in ferromagnetic and antiferromagnetic systems *Rev. Mod. Phys.* **91** 035004
- [4] Banerjee A *et al* 2016 Proximate Kitaev quantum spin liquid behaviour in a honeycomb magnet *Nat. Mater.* **15** 733–40
- [5] Nayak C, Simon S H, Stern A, Freedman M and Das Sarma S 2008 Non-Abelian anyons and topological quantum computation *Rev. Mod. Phys.* **80** 1083–159
- [6] John R and Merlin B 2016 Theoretical investigation of structural, electronic, and mechanical properties of two dimensional C, Si, Ge, Sn *Cryst. Struct. Theor. Appl.* **5** 43–55
- [7] Ding W, Zhu J, Wang Z, Gao Y, Xiao D, Gu Y, Zhang Z and Zhu W 2017 Prediction of intrinsic two-dimensional ferroelectrics in In_2Se_3 and other $\text{III}_2\text{–VI}_3$ van der Waals materials *Nature Communications* **8** 14956
- [8] Zhong H, Huang K, Yu G and Yuan S 2018 Electronic and mechanical properties of few-layer borophene *Phys. Rev. B* **98** 054104
- [9] Zhang W-B, Qu Q, Zhu P and Lam C-H 2015 Robust intrinsic ferromagnetism and half semiconductivity in stable two-dimensional single-layer chromium trihalides *J. Mater. Chem. C* **3** 12457–68
- [10] Huang B *et al* 2017 Layer-dependent ferromagnetism in a van der Waals crystal down to the monolayer limit *Nature* **546** 270–3
- [11] Liu J, Sun Q, Kawazoe Y and Jena P 2016 Exfoliating biocompatible ferromagnetic Cr–trihalide monolayers *Phys. Chem. Chem. Phys.* **18** 8777–84
- [12] Lado J L and Fernández-Rossier J 2017 On the origin of magnetic anisotropy in two dimensional CrI_3 *2D Mater.* **4** 035002
- [13] Zheng F, Zhao J, Liu Z, Li M, Zhou M, Zhang S and Zhang P 2018 Tunable spin states in the two-dimensional magnet CrI_3 *Nanoscale* **10** 14298–303
- [14] Moaied M, Lee J and Hong J 2018 A 2D ferromagnetic semiconductor in monolayer Cr–trihalide and its Janus structures *Phys. Chem. Chem. Phys.* **20** 21755–63
- [15] Webster L and Yan J-A 2018 Strain-tunable magnetic anisotropy in monolayer CrCl_3 , CrBr_3 , and CrI_3 *Phys. Rev. B* **98** 144411
- [16] Besbes O, Nikolaev S, Meskini N and Solovyev I 2019 Microscopic origin of ferromagnetism in the trihalides CrCl_3 and CrI_3 *Phys. Rev. B* **99** 104432
- [17] Zhao Y, Lin L, Zhou Q, Li Y, Yuan S, Chen Q, Dong S and Wang J 2018 Surface vacancy-induced switchable electric polarization and enhanced ferromagnetism in monolayer metal trihalides *Nano Lett.* **18** 2943–9
- [18] Lu A-Y *et al* 2017 Janus monolayers of transition metal dichalcogenides *Nat. Nanotechnol.* **12** 744
- [19] Zhang F, Mi W and Wang X 2020 Spin-dependent electronic structure and magnetic anisotropy of 2D ferromagnetic Janus $\text{Cr}_2\text{I}_3\text{X}_3$ ($X = \text{Br}, \text{Cl}$) monolayers *Adv. Electron. Mater.* **6** 1900778
- [20] Xu C, Feng J, Prokhorenko S, Nahas Y, Xiang H and Bellaiche L 2020 Topological spin texture in Janus monolayers of the chromium trihalides $\text{Cr}(\text{I},\text{X})_3$ *Phys. Rev. B* **101** 060404
- [21] Mermin N D and Wagner H 1966 Absence of ferromagnetism or antiferromagnetism in one- or two-dimensional isotropic Heisenberg models *Phys. Rev. Lett.* **17** 1133–6
- [22] Blügel S and Bihlmayer G 2007 Magnetism of low-dimensional systems: theory *Handbook of Magnetism and Advanced Magnetic Materials* (New Jersey: Wiley)

- [23] Stöhr J and Siegmann H C 2006 *Magnetism from Fundamentals to Nanoscale Dynamics* (Berlin: Springer) pp 207–504
- [24] Wu R 2007 Theory of magnetocrystalline anisotropy and magnetoelasticity in transition-metal systems. *Handbook of Magnetism and Advanced Magnetic Materials* (New Jersey: Wiley)
- [25] Johari P and Shenoy V B 2012 Tuning the electronic properties of semiconducting transition metal dichalcogenides by applying mechanical strains *ACS Nano* **6** 5449–56
- [26] Desai S B, Seol G, Kang J S, Fang H, Battaglia C, Kapadia R, Ager J W, Guo J and Javey A 2014 Strain-induced indirect to direct bandgap transition in multilayer WSe₂ *Nano Lett.* **14** 4592–7
- [27] Wang Y, Wang S-S, Lu Y, Jiang J and Yang S A 2016 Strain-induced isostructural and magnetic phase transitions in monolayer MoN₂ *Nano Lett.* **16** 4576–82
- [28] Zhang P, Peng X L, Qian T, Richard P, Shi X, Ma J Z, Fu B B, Guo Y L, Han Z Q, Wang S C, Wang L L, Xue Q K, Hu J P, Sun Y J and Ding H 2016 Observation of high-*T_c* superconductivity in rectangular FeSe/SrTiO₃ (110) monolayers *Phys. Rev. B* **94** 104510
- [29] Wang Z, Shen Y, Ito Y, Zhang Y, Du J, Fujita T, Hirata A, Tang Z and Chen M 2018 Synthesizing 1*T*–1*H* two-phase Mo_{1-x}W_xS₂ monolayers by chemical vapor deposition *ACS Nano* **12** 1571–9
- [30] Dadgar A M, Scullion D, Kang K, Esposito D, Yang E H, Herman I P, Pimenta M A, Santos E-J G and Pasupathy A N 2018 Strain engineering and Raman spectroscopy of monolayer transition metal dichalcogenides *Chem. Mater.* **30** 5148–55
- [31] Abramchuk M, Jaszewski S, Metz K R, Osterhoudt G B, Wang Y, Burch K S and Tafti F 2018 Controlling magnetic and optical properties of the van der Waals crystal CrCl_{3-x}Br_x via mixed halide chemistry *Adv. Mater.* **30** 1801325
- [32] McGuire M A, Dixit H, Cooper V R and Sales B C 2015 Coupling of crystal structure and magnetism in the layered, ferromagnetic insulator CrI₃ *Chem. Mater.* **27** 612–20
- [33] Wang H, Eyert V and Schwingenschlögl U 2011 Electronic structure and magnetic ordering of the semiconducting chromium trihalides CrCl₃, CrBr₃, and CrI₃ *J. Phys.: Condens. Matter* **23** 116003
- [34] Liechtenstein A I, Anisimov V I and Zaanen J 1995 Density-functional theory and strong interactions: orbital ordering in Mott–Hubbard insulators *Phys. Rev. B* **52** R5467–70
- [35] Ming X, Autieri C, Yamauchi K and Picozzi S 2017 Role of square planar coordination in the magnetic properties of Na₄IrO₄ *Phys. Rev. B* **96** 205158
- [36] Bruno P 1989 Tight-binding approach to the orbital magnetic moment and magnetocrystalline anisotropy of transition-metal monolayers *Phys. Rev. B* **39** 865–8
- [37] Zhou J and Huang R 2008 Internal lattice relaxation of single-layer graphene under in-plane deformation *J. Mech. Phys. Solids* **56** 1609–23
- [38] Hu Q, Wu Q, Ma Y, Zhang L, Liu Z, He J, Sun H, Wang H-T and Tian Y 2006 First-principles studies of structural and electronic properties of hexagonal BC₅ *Phys. Rev. B* **73** 214116
- [39] Lee C, Wei X, Kysar J W and Hone J 2008 Measurement of the elastic properties and intrinsic strength of monolayer graphene *Science* **321** 385–8
- [40] Landau L D and Lifshitz E M 1986 *Theory of Elasticity* (New York, NY: Pergamon)
- [41] Booth T J, Blake P, Nair R R, Jiang D, Hill E W, Bangert U, Bleloch A, Gass M, Novoselov K S, Katsnelson M I and Geim A K 2008 Macroscopic graphene membranes and their extraordinary stiffness *Nano Lett.* **8** 2442–6
- [42] Averill B and Eldredge P 2011 *General Chemistry: Principles, Patterns, and Applications* (Washington, DC: Saylor Foundation)
- [43] Goodenough J B 1963 *Magnetism and the Chemical Bond* (New York: Interscience)
- [44] Kresse G, Marsman M and Furthmüller J 2018 *VASP the Guide* (Vienna: IAEA) p 123
- [45] Wang D-S, Wu R and Freeman A J 1993 First-principles theory of surface magnetocrystalline anisotropy and the diatomic-pair model *Phys. Rev. B* **47** 14932–47
- [46] Webster L and Yan J-A 2018 Strain-tunable magnetic anisotropy in monolayer CrCl₃, CrBr₃, and CrI₃ *Phys. Rev. B* **98** 144411
- [47] Zhong D, Seyler K L, Linpeng X, Cheng R, Sivadas N, Huang B, Schmidgall E, Taniguchi T, Watanabe K, McGuire M A, Yao W, Xiao D, Fu K-M C and Xu X 2017 Van der Waals engineering of ferromagnetic semiconductor heterostructures for spin and valleytronics *Sci. Adv.* **3** e1603113
- [48] Katmis F, Lauter V, Nogueira F S, Assaf B A, Jamer M E, Wei P, Satpati B, Freeland J W, Eremin I, Heiman D, Jarillo-Herrero P and Moodera J S 2016 A high-temperature ferromagnetic topological insulating phase by proximity coupling *Nature* **533** 513
- [49] Kim J, Kim K-W, Wang H, Sinova J and Wu R 2017 Understanding the giant enhancement of exchange interaction in Bi₂Se₃–EuS heterostructures *Phys. Rev. Lett.* **119** 027201
- [50] Heide M, Bihlmayer G and Blügel S 2008 Dzyaloshinskii–Moriya interaction accounting for the orientation of magnetic domains in ultrathin films: Fe/W(110) *Phys. Rev. B* **78** 140403
- [51] Zimmermann B, Heide M, Bihlmayer G and Blügel S 2014 First-principles analysis of a homochiral cycloidal magnetic structure in a monolayer Cr on W(110) *Phys. Rev. B* **90** 115427
- [52] Kresse G and Joubert D 1999 From ultrasoft pseudopotentials to the projector augmented-wave method *Phys. Rev. B* **59** 1758–75
- [53] Blöchl P E 1994 Projector augmented-wave method *Phys. Rev. B* **50** 17953–79
- [54] Dudarev S L, Botton G A, Savrasov S Y, Humphreys C J and Sutton A P 1998 Electron-energy-loss spectra and the structural stability of nickel oxide: An LSDA+U study *Phys. Rev. B* **57** 1505–9